THE EVOLUTION, DYNAMICS AND STRUCTURE OF A NUMERICALLY MODELED LARGE DUST STORM ON MARS

S. C. R. Rafkin, *Southwest Research Institute, Boulder, CO, USA (Rafkin.swri@gmail.com)*, **J. Pla-Garcia**, *Centro de Astrobiologia, Torrejon de Ardoz, Spain; Southwest Research Institute, Boulder, CO USA; Space Science Institute, Boulder, CO USA.*

Introduction:

There have never been in situ observations at or near the active lifting center of a regional or larger dust storm on Mars. Landed meteorological packages have recorded the atmospheric environment during large and global dust storms, but only at a distance from the presumed active areas. As a general rule, an increase in local dust opacity from a distant dust storm results in an overall decrease in the amplitude of the diurnal thermal cycle in the atmosphere and at the surface; overnight minimum temperatures increase and daytime maximum temperatures decrease [Wilson and Richardson, 2000; Ryan and Henry, 1979]. The pressure cycle is also usually perturbed, with an increase in the semi-diurnal cycle being a common effect [Leovy and Zurek, 1979].

In the absence of in situ data, it is common to employ numerical models to provide guidance on the physical processes and conditions operating in an unobserved location or weather system. This is a reasonable approach assuming the model has been adequately validated at other locations. Toigo et al [2005] was the first to model mesoscale dust storm systems. Looking exclusively at high northern latitudes and polar cap edge storms, Toigo et al. found that dust essentially behaved as a passive tracer. Lower latitude dust storms and disturbances have been modeled under idealized conditions (Rafkin 2009; Spiga et al, 2013]. These showed greater amounts of dust-radiation-dynamic feedback. Rafkin [2009] attributes this to the greater solar forcing at lower latitudes. Several studies have modeled dust storms on the large scale, but only for the purpose of trying to simulate the mean global dust cycle or to understand the stochastic nature of dust storms [Basu et al., 2004; Basu et al. 2006; Kahre et al. 2006; Newman et al., 2002]. The GCMs in these studies are, by design, unable to simulate detailed mesoscale (or smaller structures). Here, the dynamics and conditions in the vicinity of the active lifting region of a large dust storm modeled under realistic forcing conditions are discussed.

Numerical Experiment:

In support of the Mars 2020 Rover mission (hereafter M2020), mesoscale modeling of 11 landing sites with high science potential have been modeled to characterize and identify possible hazardous atmospheric conditions during entry, descent and landing (EDL) operations. This exercise is similar to that performed for previous missions [e.g., Rafkin and Michaels, 2003; Tamppari et al, 2008; Vasavada et al., 2012]. M2020 will land at Ls ~5, a season in which local to large-scale dust storms are climatological possible. Consequently, substantial effort has gone into simulating both nominal (non-dust storm) conditions as well as those conditions that might be expected in a dust storm. For the purposes of this study, the results of dust storm scenarios in the vicinity of the landing sites at Syrtis (lat/lon) and Jezero Crater (lat/lon) are presented.

One method to investigate dust storm conditions is to utilize a fully interactive dust cycle. In this scenario, surface winds are allowed to lift dust, the lifted dust is permitted to radiatively pertub the thermal structure of the atmosphere, and the dynamics (the winds) evolve and transport the lifted dust according to the radiative forcing. The advantage of this technique is that it fully captures the feedback loop (positive or negative) between dynamics, dust distribution and radiative forcing. Based on previous modeling work, this feedback is thought to be important for a range of dust disturbances [Rafkin 2009]. The disadvantage of this technique is that the precise location, trajectory, dust distribution, and overall evolution of the dust storm cannot be fully controlled or prescribed. Additionally, dust lifting parameters—the minimum surface wind stress lifting threshold and the dust lifting efficiency—must be tuned to reproduce the desired spatial and temporal extent of the storm, as well as the overall magnitude.

The lifting threshold controls the location and extent of the source regions of the dust. The lower the threshold, the greater the area of dust lifting that will be activated. The efficiency throttles the magnitude of the dust flux into the atmosphere at active lifting sites. For a fixed lifting threshold, the efficiency is the dominant parameter in determining the total amount of dust injected into the atmosphere.

The tuning required to generate a desired dust storm scenario may be outside the bounds of reasonable physics and, when improperly set, could result in nonphysical dust storm scenarios. For example, if modeled wind stresses are very low, the lifting threshold may need to be set to unreasonably small values in order to produce a sufficiently large dust lifting area. Likewise, it may be necessary to increase the efficiency parameter to an unrealistically

large value in order to produce reasonable dust column opacities within the storm. Conversely, some combinations of threshold and efficiencies could result in a dust storm with absurd opacities (e.g., >100) or active dust lifting nearly everywhere within the modeling domain.

The Mars Regional Atmospheric Modeling System (MRAMS [Rafkin et al., 2001]) is employed for this study. MRAMS is highly flexible in the way it can handle atmospheric dust. In the present configuration, the model is configured with two independent dust fields. The first dust field is used to capture and represent the effects of the typical, climatological dust loading. This dust field, known as the background dust, is specified according to representative climatological values of dust as determined from the Mars Global Surveyor Thermal Emission Spectromter (TES). The vertical distribution of background dust is specified using a Conrath-ν profile that is a function of latitude and season. The background dust field is always radiatively active, and evolves slowly in time according to climatological parameters. The second dust field, known as foreground dust, is populated by dust lifted off the surface. Foreground dust evolves according to the model-predicted winds and diffusion. Foreground dust also undergoes sedimentation according to size dependent and atmospheric density dependent fall velocity. It is the foreground dust that can produce a dust storm, and the foreground dust field is superimposed on the background dust field; the total dust content is a sum of the background and foreground dust field. Foreground dust can be radiatively active or passive.

The simulation has five grids (Figure 1), and dust lifting is permitted only on grids two through five. Limiting the dust lifting to the four highest resolution grids forces the model to produce a dust storm no larger than the size of the third grid domain. The simulation is run for a total of five sols with the simulations starting at ~0000 (local time). Dust lifting is activated at ~1900 local, and continues through sol 2 and sol 3. Lifting is deactivated on sol 4 in order to force dust storm decay.

Results: During the afternoon on the sol 2, the first day of dust lifting, two primary areas of lifting develop (Fig. 2). The first area is in the northeast region of the grid, and is already organized into a linear feature that becomes more disorganized through the day. The second area is on the southeast rim of the Syrtis impact basin. The Syrtis area organizes into a linear feature roughly aligning with the daytime upslope flow.

A cross-section showing different atmospheric fields at x=85 and ~1400 local is displayed in Fig. 3. The dust mixing ratio shows a deep (> 6 km) plume just to the north of the Isidis crater rim. The mixing

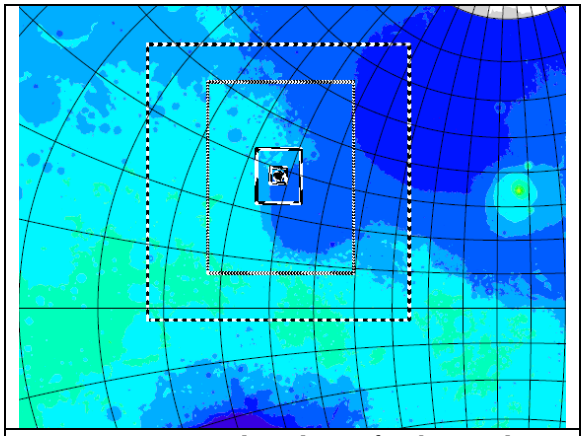

Figure 1. Numerical Grids 2-7 for the simulation of the 2020 Jezero Crater landing site. Only grids 1-5 are used in the dust storm simulation, and dust lifting is permitted only on grids 2-5.

ratio peaks near the surface and drops off with height. This dust profile is consistently seen in active lifting regions. The surface maximum is partly due to the surface being the source of dust, with entrainment of less dusty air as the plume rises. However, it is also because the mixing ratio can be dominated by a few large dust aerosol, since the mass is proportional to the cubed of the radius. Dust lifted off the surface is assumed to follow a log-normal distribution, which includes a few large particles. Once lifted, the largest dust tends to sediment out while the smaller dust continues to be advected upward by the plume. This size-sorting process tends to drive the mixing ratio profile to a maximum near the surface.

In the plume near the surface, the air temperature is as much as 20K colder than nearby areas. This is due to solar absorption higher in the dust

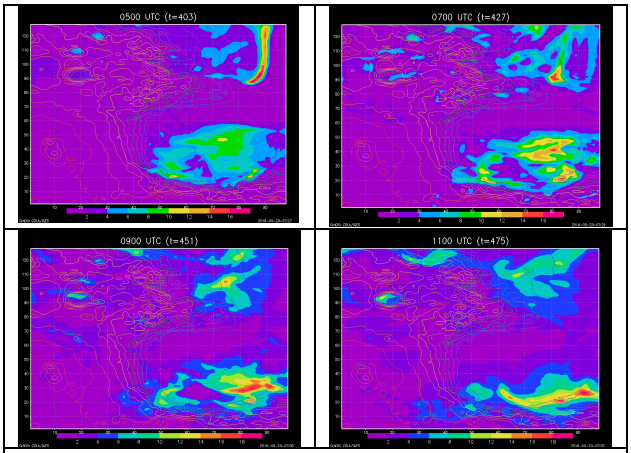

Figure 2. Column visible dust opacity (shaded) and topography (contours) on grid 3 during the afternoon. Times are given in Mars UTC. Add ~5 hours for local time. Axes are labelled by grid point (~27 km spacing).

column limiting direct heating deeper into the atmosphere. Overall, within the plume, there is an inversion, and although the top of the plume is warmer than below, it is near neutral buoyancy com-

pared to the less dusty air on either side. Apparently, adiabatic cooling nearly offsets the expected positive heating perturbation at the top of the dusty plume.

Turbulent kinetic energy is confined to a much shallower layer near the surface in and around the dust plume. This structure is consistent with the thermal structure—an inversion—that will tend to suppress buoyancy of generation of turbulence. In contrast, near the middle of the grid where a more traditional steep lapse rate is present, deep convective, but non-dusty plumes are present.

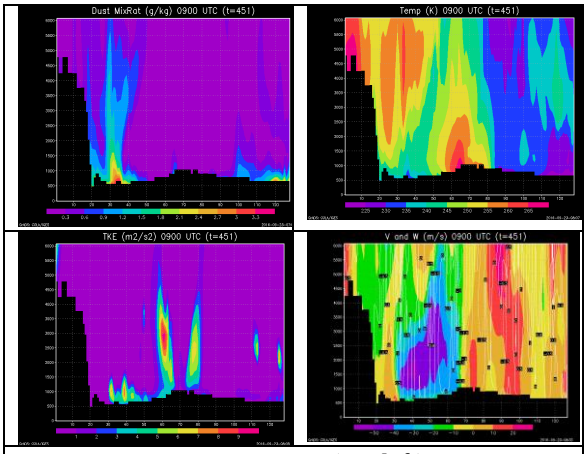

Figure 3. Dust mixing ratio (top left), temperature (top right), Turbulent kinetic energy (bottom left) and v (shaded) and w (contoured) wind (bottom right) on grid 3 at x=85 during the afternoon.

Finally, a very strong (>60 m/s) low level jet forms in the vicinity of the dusty plume. This structure results entirely from the dust storm distribution, which can be seen by examining the model solution when lifted dust (foreground dust) is not radiatively active (Fig. 4).

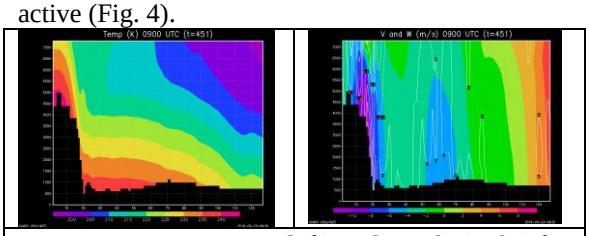

Figure 4. Temperature (left) and winds (right) for the same cross-section as in Figure 3, but for the case of radiatively passive dust.

Summary and Conclusions: Large dust storms have a profound effect on the immediate atmospheric environment. The atmospheric structure exhibits large variability and the structure deviates substantially from the broad thermal stabilization and ampflication of the Hadley Cell and thermal tide signature. There is substantial feedback between the dust and dynamics. The development of the strong low level jet is sufficient to increase the surface stress and enhance dust lifting. This is contrast to the limited feedback found by Toigo et al (2002) for polar cap edge storms. The discrepancy is very likely due to the very different conditions between the polar cap edge storms and the lower latitude storm simulated here.

Orbital images of dust storms frequently show textured, convective looking features at the top of the storm. This is consistent with the dusty plumes and high spatial heterogeneity found in the numerical simulations. However, the turbulent kinetic energy fields suggest that smaller-scale turbulence may be suppressed nearby high column opacity regions. The depth of the convective boundary layer is also reduced.

The most well defined dust plumes do not show excessive thermal buoyancy. Instead, the adiabatic cooling from the rising plume roughly offsets the diabatic heating. This near neutral buoyancy is in contrast to the rocket dust storm concept of Spiga et al [2013] where neutral buoyancy is only achieved once the dust has been substantially diffused or when solar heating ceases.

The simulations also show that dust is not close to being well mixed in the central regions of a dust storm. Generally, there is a maximum of dust mixing ratio in the lower levels. Farther away from the active regions, detached dust layers are often found. These layers are the result of the advection of dust that has been expelled and detrained from dusty plumes farther upwind.

In conclusion, the conditions within the active region of a storm are highly dynamic and highly dynamic. Both the thermal and kinematic structure are highly perturbed. A fully interactive dust cycle is likely necessary to capture the full dynamic range within storms. In situ surface measurements are needed to validate the actual conditions within a storm.

References:

Basu, S., Richardson, M. I., & Wilson, R. J. (2004). Simulation of the Martian dust cycle with the GFDL Mars GCM. Journal of Geophysical Research: Planets, 109(E11).

Basu, S., Wilson, J., Richardson, M., & Ingersoll, A. (2006). Simulation of spontaneous and variable global dust storms with the GFDL Mars GCM. Journal of Geophysical Research: Planets, 111(E9).

Kahre, M. A., Murphy, J. R., & Haberle, R. M. (2006). Modeling the Martian dust cycle and surface dust reservoirs with the NASA Ames general circulation model. Journal of Geophysical Research: Planets, 111(E6).

Leovy, C. B., & Zurek, R. W. (1979). Thermal tides and Martian dust storms: Direct evidence for coupling. Journal of Geophysical Research: Solid Earth, 84(B6), 2956-2968.

Newman, C. E., Lewis, S. R., Read, P. L., & Forget, F. (2002). Modeling the Martian dust cycle, 1.

Representations of dust transport processes. Journal of Geophysical Research: Planets, 107(E12).

Rafkin, S. C., Haberle, R. M., & Michaels, T. I. (2001). The Mars regional atmospheric modeling system: Model description and selected simulations. Icarus, 151(2), 228-256.

Rafkin, S. C., & Michaels, T. I. (2003). Meteorological predictions for 2003 Mars Exploration Rover high-priority landing sites. Journal of Geophysical Research: Planets, 108(E12).

Rafkin, S. C. (2009). A positive radiative-dynamic feedback mechanism for the maintenance and growth of Martian dust storms. Journal of Geophysical Research: Planets, 114(E1).

Ryan, J. A., & Henry, R. M. (1979). Mars atmospheric phenomena during major dust storms, as measured at surface. Journal of Geophysical Research: Solid Earth, 84(B6), 2821-2829.

Spiga, A., Faure, J., Madeleine, J. B., Määttänen, A., & Forget, F. (2013). Rocket dust storms and detached dust layers in the Martian atmosphere. Journal of Geophysical Research: Planets, 118(4), 746-767.

Tamppari, L. K., Barnes, J., Bonfiglio, E., Cantor, B., Friedson, A. J., Ghosh, A., ... & Michaels, T. (2008). Expected atmospheric environment for the Phoenix landing season and location. Journal of Geophysical Research: Planets, 113(E3).

Toigo, A. D., Richardson, M. I., Wilson, R. J., Wang, H., & Ingersoll, A. P. (2002). A first look at dust lifting and dust storms near the south pole of Mars with a mesoscale model. Journal of Geophysical Research: Planets, 107(E7).

Vasavada, A. R., Chen, A., Barnes, J. R., Burkhart, P. D., Cantor, B. A., Dwyer-Cianciolo, A. M., ... & Lewis, S. R. (2012). Assessment of environments for Mars Science Laboratory entry, descent, and surface operations. Space science reviews, 170(1-4), 793-835.

Wilson, R. J., & Richardson, M. I. (2000). The Martian atmosphere during the Viking mission, I: Infrared measurements of atmospheric temperatures revisited. Icarus, 145(2), 555-579.

Acknowledgements: The initial work presented here was supported by a contract under the Mars Critic Data Program. Follow on work as supported by the NASA SSW Program.